Article

BAY-7081: A Potent, Selective, and Orally Bioavailable Cyanopyridone-Based PDE9A Inhibitor

Daniel Meibom,* Sina Micus, Anna Lena Andreevski, Sonja Anlauf, Pamela Bogner,
Clemens-Jeremias von Buehler, André P. Dieskau, Jan Dreher, Frank Eitner, Daniela Fliegner,
Markus Follmann, Kersten Matthias Gericke, Stefanie Maassen, Jutta Meyer, Karl-Heinz Schlemmer,
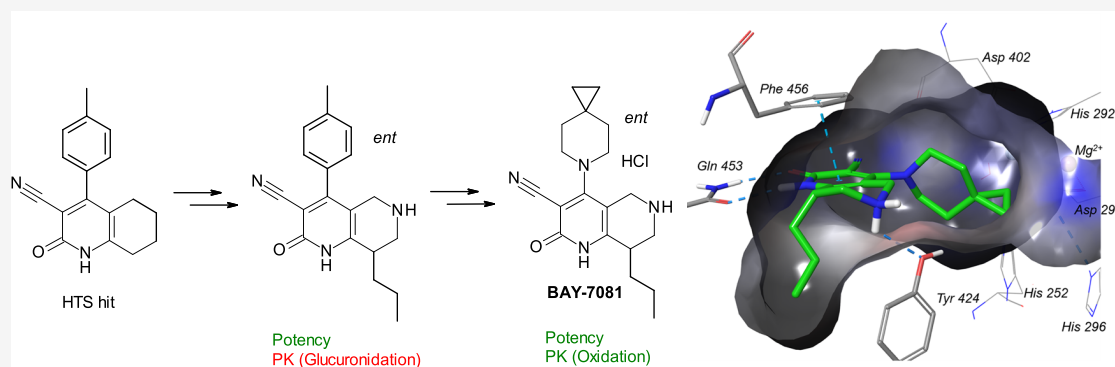Holger Steuber, Adrian Tersteegen, and Frank Wunder

Read Online

ACCESS | Metrics & More | Article Recommendations | Supporting Information

ABSTRACT: Despite advances in the treatment of heart failure in recent years, options for patients are still limited and the disease is associated with considerable morbidity and mortality. Modulating cyclic guanosine monophosphate levels within the natriuretic peptide signaling pathway by inhibiting PDE9A has been associated with beneficial effects in preclinical heart failure models. We herein report the identification of BAY-7081, a potent, selective, and orally bioavailable PDE9A inhibitor with very good aqueous solubility starting from a high-throughput screening hit. Key aspect of the optimization was a switch in metabolism of our lead structures from glucuronidation to oxidation. The switch proved being essential for the identification of compounds with improved pharmacokinetic profiles. By studying a tool compound in a transverse aortic constriction mouse model, we were able to substantiate the relevance of PDE9A inhibition in heart diseases.

INTRODUCTION

One of the most important intracellular second messengers in mammalian cells is cyclic guanosine monophosphate (cGMP). Together with nitric oxide (NO), which is released by the vascular endothelium, and soluble guanylate cyclase (sGC), it forms the NO/sGC/cGMP signaling cascade.[1] cGMP levels are regulated by the synthesis rates of soluble and particulate guanylate cyclases and the degradation rates of cGMP-hydrolyzing phosphodiesterases (PDEs).[2] Eleven PDE iso-enzymes are known, which are located in various human tissues.[3,4] PDE9A, a very high-affinity cGMP-specific PDE which is believed to be a key regulator of cGMP levels,[5,6] is highly expressed in the kidney, brain, and spleen[7−10] and to some extent in the heart.[11]

The formation of cGMP and the resulting regulation of PDEs, ion channels, and protein kinases play a decisive role in different physiological processes, in particular for the relaxation and proliferation of smooth muscle cells, the proliferation of fibroblasts, and platelet aggregation and adhesion.[1] Under

conditions of pathophysiology, the cGMP system can be suppressed, leading to, for example, kidney diseases,[12,13] cardiac insufficiency,[14,15] hypertension, arteriosclerosis, thrombosis, and sexual dysfunction.[16,17] A treatment option for cardiovascular diseases such as chronic kidney disease and heart failure by inhibiting PDE9A may represent a promising approach on account of the physiological importance of cGMP and expected lack of hemodynamic effects.

To date, the chemical structures of various preclinical and clinical PDE9A inhibitors, most of them for the treatment of the central nervous system (CNS) disorders and sickle cell disease, have been published.[18−21] Recently, heart failure has
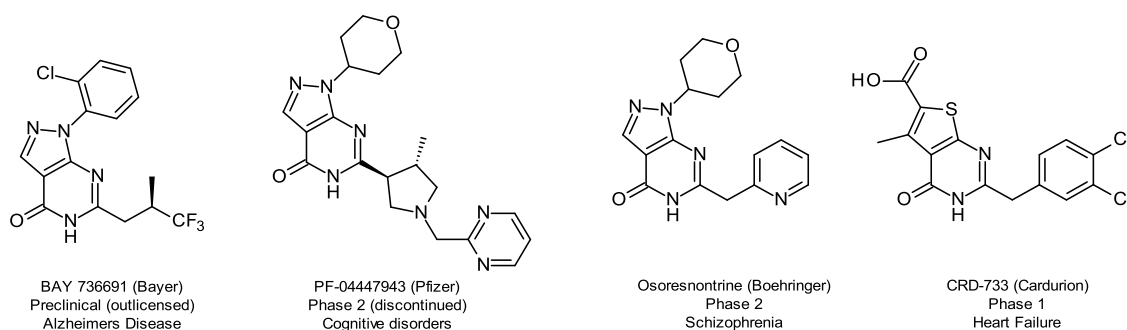
Figure 1. Examples of publicly known PDE9A inhibitors.

been discussed in the literature as a potential indication for PDE9A inhibitors as well.[22,23] Small biotechs (e.g., Cardurion, Figure 1) are currently evaluating their assets for the treatment of heart failure with reduced (HFrEF) and preserved ejection fraction (HFpEF). Figure 1 exemplifies inhibitors employing a pyrimidinone core with an anellated five-membered hetero-cycle, a motif frequently used in the PDE9A field.[24−26]

With BAY-7081, we herein report the successful identi-fication of a new potent, selective, and soluble cyanopyridone-based PDE9A inhibitor chemotype which necessitated optimization toward reduced glucuronidation to achieve improved pharmacokinetic (PK) profiles.

RESULTS AND DISCUSSION

Optimization of Potency. Cyanopyridone **1** was identi-fied as a moderately active inhibitor of human PDE9A (Table 1) by a cell-based high-throughput screening (HTS) campaign using a recombinant PDE9A reporter cell line[24] and Bayer's small-molecule compound library. No activities versus PDE2A to PDE5A, PDE7B, PDE8A, and PDE10A were observed for **1**. However, **1** was found to be unselective against bovine brain PDE1 and PDE11A while showing only 17-fold selectivity versus bovine retinal PDE6. Our first goal in optimizing the HTS hit was to achieve increased potency. Docking **1** into a publicly available X-ray structure of human PDE9A (PDB: 3JSW) proposed important interactions to already be in place. The cyclic lactam of **1** potentially forms H-bonds with Gln453 of the protein, while the pyridone core might make use of π-stacking with Phe456. Furthermore, a cavity in the GTP-binding site seems to accommodate the tolyl moiety. However, a lipophilic pocket which should be addressable by substituents in position C-8 of the lead structure was not yet leveraged by the HTS hit (Figure 2).

We were pleased to see that adding a simple methyl group already improved IC_{50} by a factor of 2 (Table 1, **2**). According to the above-mentioned modeling studies, only one of the two stereoisomers should be able to fill the pocket and thus be active. Consequently, the enantiomer of **2** inhibited PDE9A with an IC_{50} of only 16 μM. Further potency improvement was achieved with an ethyl substituent (**3**), while the optimum was reached with propyl (**5**). Branching like in **4** or **7** elevated the IC_{50} as well as increasing steric bulk (**8**) or chain length (**9**). Incorporation of polar substituents into the C8 side chain was not tolerated (data not shown). However, ethers like in **6** were compatible with potency.
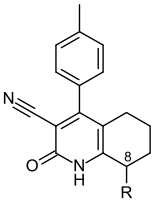
Optimization of Selectivity and Solubility. Character-izing PDE selectivity (PDE1-PDE11) of the propyl derivative **5** yielded good to very good selectivity factors of at least 69-fold except for PDE1. Here, the inhibitor was only fivefold more

potent versus PDE9A. Again, docking provided guidance for further optimization. As visible in Figure 3, interaction with tyrosine 424 (which is exchanged for a phenylalanine in PDE1) was proposed. Hydrogen bonding of the phenolic oxygen of Tyr424 with an amino functionality placed within the cyclohexene ring was envisioned. Incorporation of a polar group should at the same time improve solubility in aqueous media, which was undetectable for the propyl-substituted cyanopyridone **5**.

Table 2 shows that a nitrogen atom in position C-6 improved selectivity versus PDE1 and solubility with only little decrease in potency versus PDE9A (**13**). If these effects can be attributed to hydrogen bonding remains speculative. An alternative explanation could be that the more polar environ-ment imparted by the amine nitrogen in the cyclohexene ring disfavors binding of **13** close to the lipophilic Phe392 of PDE1. PDE2A to PDE8A, PDE10A, and PDE11A were not significantly inhibited by **13** at concentrations below 5 μM. Placing the amino nitrogen in position C-5 or C-7 yielded compounds with reduced potency (**11** and **12**).

In a chemical subseries with alkylation at the nitrogen in position 6, we validated our modeling approach by obtaining an X-ray cocrystal structure of inhibitor **13A** with PDE9A. Key interactions were visible: the cyclic lactam of **13A** forms H-bonds with Gln453, π-stacking between the pyridone and Phe456 takes place, and the propyl side chain accommodates in a lipophilic pocket (Figure 4), distributed over multiple conformational states. The stereocenter is S configured. No H-bond was found between the nitrogen in position 6 of inhibitor **13A** and Tyr424. Instead, the distance between the carbonyl oxygen of the amide containing side chain and the phenolic oxygen of Tyr424 suggests the formation of an H-bond in **13A**. However, in other cases, a direct polar interaction of the core nitrogen with Tyr424 might become possible, for example, due to rotational freedom of the tyrosine. As a consequence of poor PK properties resulting from N-dealkylation, the chemical subseries was not further pursued.

Optimization of PK. After iv and oral administration of **13** to rats, high clearance, low mean residence time, and low bioavailability were observed (Cl_{bl} 3.6 L/kg/h, MRT_{iv} 0.8 h, and F 15%). The low metabolic stability could be attributed to extensive phase-II metabolism (see the Supporting Informa-tion) as incubation with rat and human hepatocytes showed quick and almost complete glucuronidation of the cyclic lactam of **13**. Several strategies were evaluated to reduce glucur-onidation. Increasing steric bulk close to the pyridone NH moiety (**14**), employing an intramolecular hydrogen bond (**15**), alkylating the pyridone NH (**16**), as well as changing the core (**17**) all met with failure, as can be seen from Figure 5.

## Table 1. Exploration of C8 Structure−Activity Relationship (SAR) to Improve Potency vs PDE9A[a]

Compound	R	IC$_{50}$ [nM][a]
1$_{(ent)}$	H	530
2$_{(ent)}$	Me	220
3$_{(ent)}$	Me	60
4$_{(ent)}$	Me, Me	130
5$_{(ent)}$	Me	10
6$_{(ent)}$	O, Me	85
7$_{(ent)}$	Me, Me	25
8$_{(ent)}$	CF$_3$	140
9$_{(rac)}$	Me	35

[a]IC$_{50}$ versus human PDE9A was measured with a scintillation proximity assay using ^{3}H-cGMP as the substrate (see the Supporting Information); ent: single enantiomer, absolute stereochemistry was not elucidated; rac: racemate.

Next, we followed the idea to influence overall metabolic stability by increasing polarity. Therefore, various electron-withdrawing head groups were screened. However, none of the resulting compounds were sufficiently potent. Table 3 shows some of the most active examples that were identified.

At that point, we revisited an alternative screening hit (**24**, Figure 6) belonging to a subseries where we struggled to achieve potent PDE9A inhibition (e.g., **25**).

At the time of the lead optimization phase, to the best of our knowledge, it was not publicly known that **24** is a PDE9A
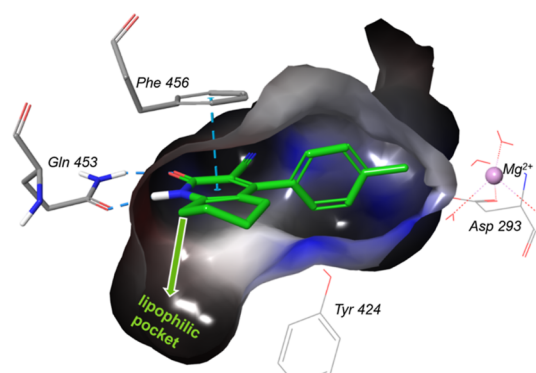
Figure 2. Docking of screening hit **1** into human PDE9A X-ray (PDB: 3JSW) and visualization of lipophilic pocket to be addressed with substituents in position 8.
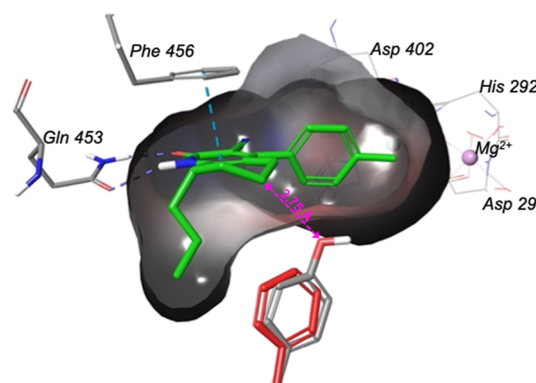
Figure 3. Docking of **5** into human PDE9A X-ray (PDB: 3JSW) and overlay with human PDE1B X-ray (PDB: 1TAZ). Visualization of Tyr424 which might be addressable by H-bonding to improve selectivity vs PDE1. The distance between the phenolic oxygen of Tyr424 and an N−H in the indicated position of the six-membered ring should be smaller than 3.75 Å.

inhibitor. However, later on, others have published on the PDE9A activity of similar compounds with piperidine head groups.[27,28] The positive PK properties of **24** in rats (Cl$_{bl}$ 1.6 L/kg/h, MRT$_{iv}$ 1.3 h, and F 61%) prompted us to combine the dimethylpiperidine with the propyl-substituted core structure exemplified by **13**. The resulting molecule **27** (Figure 6) was our first cyanopyridone that showed no glucuronidation after incubation with rat hepatocytes and was thus characterized in detail (Table 4).

Compared to **13**, **27** is slightly less potent and selective, while on the other hand, in vivo PK properties in rats have slightly improved. The main clearance pathway of compound **27** is driven by oxidative metabolism (see the Supporting Information). As we had been unsuccessful in optimizing phase-two-driven metabolism, we used **27** as a new starting point to improve PK. Furthermore, very high fraction unbound in rat and human plasma (rat 41%, human 52%) gave us confidence that by starting from **27**, obtaining a PDE9A inhibitor tool compound to evaluate in vivo pharmacody-namics should be possible.

As piperidine head group SAR was largely unknown to us, we concentrated on this part of the molecule. Table 5 shows selected examples from >350 amino head groups that have been tested.

Omitting both methyl groups of **27** led to less-potent pyridone **28**. As the monomethyl analogue of **24** had an IC$_{50}$
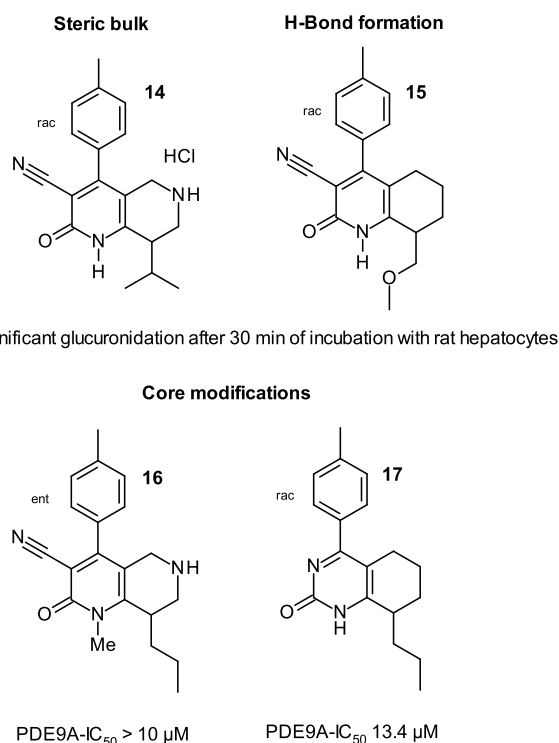
Table 2. Exploration of Position for Polar Spot

Compound	Structure	IC$_{50}$ [nM][a]	PDE1[b]	Solubility [mg/l][c]	Compound	Structure	IC$_{50}$ [nM][a]	PDE1[b]	Solubility [mg/l][c]
11(rac)					11(rac)		1500	0x	-
10(rac)		310	3x	9	12(rac)		7000	1x	-
5(ent)		10	5x	< 1	13(ent)		20	22x	331

[a]See the Supporting Information for details on measurement of IC$_{50}$ versus human PDE9A and PDE1. [b]PDE1 selectivity factors were calculated by dividing the IC$_{50}$ for PDE1 by the IC$_{50}$ for human PDE9A (PDE1-IC$_{50}$/PDE9A-IC$_{50}$). [c]Solubility at pH 6.5 (see the Supporting Information); ent: single enantiomer, absolute stereochemistry was not elucidated; rac: racemate.
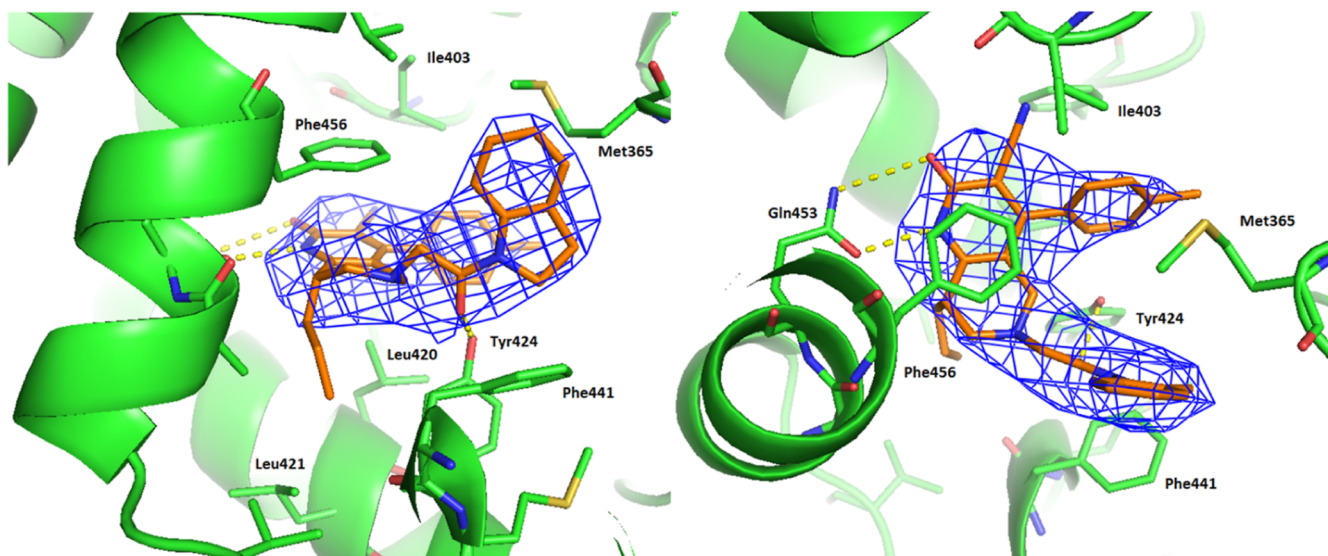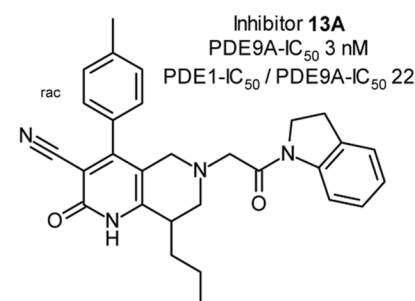
Figure 4. X-ray cocrystal structure of **13A** in PDE9A. The bound inhibitor **13A** is shown in orange, the $2F_o − F_c$ electron density at 1.0σ is represented as blue mesh. The atomic coordinates have been deposited under PDB entry 8BPY.

Steric bulk   **H-Bond formation**

Significant glucuronidation after 30 min of incubation with rat hepatocytes

Core modifications

PDE9A-IC$_{50}$ > 10 μM   PDE9A-IC$_{50}$ 13.4 μM

Figure 5. Attempts to reduce glucuronidation. See the Supporting Information for measurement of glucuronides and IC$_{50}$ vs human PDE9A; ent: single enantiomer, absolute stereochemistry was not elucidated; rac: racemate.

of only 710 nM, we opted against synthesizing the combination with the core of **13** but rather made the nitrile **29** which was the more potent headgroup in the anellated pyridine series. Unfortunately, **29** proved to be less active than **27**. As cyclopropanes can be metabolically more stable than the corresponding gem-dimethyl analogues, we synthesized inhibitor **30** (BAY-7081) and were pleased to have obtained a more potent and selective compound. By blocking potential metabolic soft spots, **31** and **32** could in principle have yielded PDE9A inhibitors with reduced clearance. However, both compounds were deprioritized because of being less potent and selective compared to **30**. The spiro cyclobutyl derivative **33** was comparable to **30**; however, it was less efficient as one additional methylene group was required for being equipotent [LLE **33**: 5.6, LLE **30**: 6.1, LLE = $-\log(\text{IC}_{50}) - c \log D_{7.5}$]. The corresponding oxetane **34** looked promising at first sight. However, **34** was inactive in a PDE9A cell-based assay[24] (EC$_{50}$ > 10 μM). Widening up the spirocycle to **35** and **36** had no advantage in terms of activity on PDE9A or selectivity versus PDE1.

The spirocyclopropyl derivative BAY-7081 (**30**) was the best compound taking biochemical and cellular potency, selectivity, and lipophilic ligand efficiency into account. Docking of **30** into PDE9A (Figure 7) shows the optimal filling of the lipophilic pocket by the propyl side chain which drives potency. In addition, interaction of the anellated piperidine NH group with tyrosine 424 is visible. As explained above, this putative hydrogen bond might be beneficial to achieve selectivity versus PDE1.

Synthesis of BAY-7081. For a detailed characterization, multigram amounts of BAY-7081 (**30**) were prepared according to Scheme 1. The commercially available piperidine

Table 3. Attempts to Improve Metabolic Stability by Employing Electron-Withdrawing Head Groups

Compound	R	IC$_{50}$ [nM][a]
18(rac)		430
19(rac)		640
20(rac)		630
21(rac)		570
22(rac)		410
23(rac)		600

[a]IC$_{50}$ versus human PDE9A was measured with a scintillation proximity assay using ^{3}H-cGMP as the substrate (see the Supporting Information); rac: racemate.
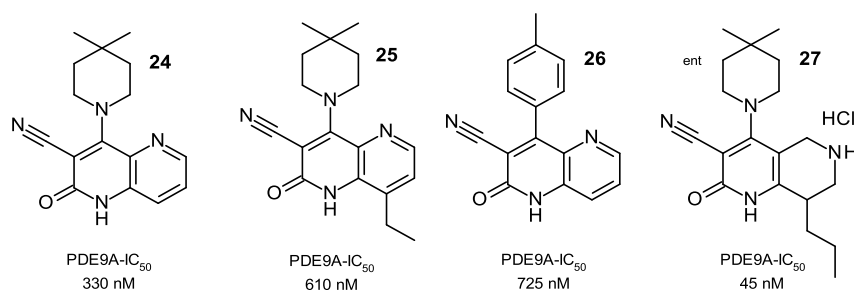
Figure 6. Alternative HTS hit series. For measurement of IC$_{50}$ versus human PDE9A, see the Supporting Information. ent: single enantiomer, absolute stereochemistry was not elucidated.

Table 4. Comparison of Compounds 13 and 27

	13	27
IC$_{50}$ [nM]^a	20	45
Selectivity factors^b	PDE1 22x, PDE2A/3B/5A/7B−11A > 100x, PDE4B > 100x, PDE6 > 100x	PDE1 13x, PDE2A/3B/5A/7B−11A ≥ 100x, PDE4B 46x, PDE6 25x
Rat PK properties^c	Cl$_{bl}$ 3.6 L/kg/h, MRT$_{iv}$ 0.8 h, F 15%	Cl$_{bl}$ 2.8 L/kg/h, MRT$_{iv}$ 1.2 h, F 25%

^{a}IC$_{50}$ versus human PDE9A enzyme, see the Supporting Information. ^{b}Selectivity factors were calculated by dividing the IC$_{50}$ of a given PDE by the human PDE9A-IC$_{50}$ (PDE#-IC$_{50}$/PDE9A-IC$_{50}$), see the Supporting Information for details on IC$_{50}$ measurements. ^{c}Values were derived by intravenous and oral administration of solutions in either plasma 99% + DMSO 1% (iv) or EtOH/PEG400/H$_2$O (po) vehicles. C$_{bl}$ blood clearance, MRT mean residence time after iv application, and F oral bioavailability (see the Supporting Information).

37 was reacted with a bis-nitrile-substituted ketene dithioacetal on a 100 g scale. **38** was obtained in high yield and reacted with the *tert*-butoxycarbonyl (BOC)-protected piperidine **41**. The latter piperidine was also prepared on a 100 g scale by alkylating the enamine of commercial **39** with allyl bromide and subsequent hydrogenation. The key step of the synthesis is the two step—one-pot cyclization[29,30] toward **42**. First, the enolate of **41** is reacted with the acrylonitrile **38** under loss of methyl mercaptan. Ring closure to assemble the pyridone motif is then achieved by heating in aqueous acetic acid. Chiral separation of the enantiomers of **42** gave **43** in very good yield (46% of theoretically possible 50%). After deprotection, more than 18 g of **30** were obtained.

Characterization of BAY-7081. Broad profiling of BAY-7081 (**30**) started by assessing its inhibitory potential versus a range of phosphodiesterases. Human PDE9A is inhibited with an IC$_{50}$ of 15 nM, while mouse and rat enzymes show 50% inhibition at concentrations of 34 and 42 nM, respectively. The distomer of **30** is inactive (hPDE9A-IC$_{50}$ > 10 μM). Compared to the PDE9A-IC$_{50}$ of BAY-7081, the IC$_{50}$ versus PDE1 is 49-fold higher, while for other phosphodiesterases, an even better selectivity factor was observed (Table 6).

In addition to the above-mentioned biochemically determined IC$_{50}$ value versus human PDE9A, we also measured potency in a cell-based assay.[24] Here, **30** showed an EC$_{50}$ of 1 μM which favorably compares to 1.7 μM for Pfizer's former PDE9A development compound PF-04447943. In vivo PK evaluation of our best PDE9A inhibitor in rats and dogs also produced encouraging results when compared to the competitor molecule (Tables 7 and 8) which has been tested as a twice daily oral drug in clinical studies.[31]

Protein binding for BAY-7081 (**30**) is low in several species including humans (fraction unbound: mouse 41%, rat 20%, dog 43%, monkey 42%, and human 34%). No inhibition of CYP1A2, 2C8, 2D6, and 3A4 enzymes was detected at 20 μM. For CYP2C9, an IC$_{50}$ of 16 μM was measured. CYP-inducing potential of **30** was assessed for CYP1A2 and 3A4. For CYP1A2, no induction was seen. However, CYP3A4 mRNA

was induced at concentrations above 9.2 μM. After incubation with rat and human hepatocytes, no reactive metabolites were formed. Furthermore, **30** is very stable in the presence of human hepatocytes and showed almost no degradation after 4 h of incubation. Evaluation of inhibition of 75 off-targets (Panlabs) and cardiac ion channels (hERG, Na$_v$1.5) revealed a clean profile. No genotoxicity was found in an Ames test.

The physicochemical characterization of the cyanopyridone **30** is in line with drug-like, rule of five compliant properties. Furthermore, high solubility from crystalline material was observed (Table 9), potentially allowing not only for oral but also for iv administration:

Pharmacodynamic Studies. PDE9A expression has been reported for various tissues including those of the kidney[7−10] and the heart.[11,32] Furthermore, the recent literature suggests that inhibiting PDE9A might be beneficial for the treatment of renal dysfunction,[33] HFrEF[34,35] and HFpEF.[36,37] We therefore studied urinary cGMP in rats and functional parameters in a rat heart failure model after PDE9A inhibition.

For cGMP measurements, rats with a bladder catheter were treated with 10 or 50 mg/kg PF-04447943 by gavage and urine was collected 85 min after dosing. Statistically significant urinary cGMP increases were seen upon PDE9A inhibition as compared to vehicle treatment (Figure 8). For BAY-7081 (**30**), a nonsignificant trend toward higher cGMP levels was observed at 40 mg/kg.

Variability in the urinary cGMP model was generally high, while signal amplitude is low. Both aspects have impacted the study with BAY-7081 in particular. Furthermore, local kidney concentrations of both compounds have not been determined and might explain the observed differences as well. More studies with higher animal numbers and higher doses are needed to solidify the impact of PDE9A inhibition on urinary cGMP. To rule out that the observed cGMP rises are secondary to blood pressure effects potentially mediated by blocking PDE9A, PF-04447943 and BAY-7081 (**30**) have been evaluated in telemetric rats. After twice daily oral administration of 10 or 50 mg/kg PF-04447943 and once daily oral

Table 5. Piperidine Head Group SAR[a]

Compound	R	IC$_{50}$ [nM][b]	PDE1[c]
27(ent)		45	13x
28(rac)		200	43x
29(rac)		92	87x
30(ent)		15	49x
31(rac)		100	9x
32(rac)		69	30x
33(ent)		13	45x
34(ent)		6	45x
35(ent)		23	39x
36(rac)		13	12x

Table 5. continued

[a]See the Supporting Information for salt forms. [b]IC$_{50}$ versus human PDE9A was measured with a scintillation proximity assay using ^{3}H-cGMP as the substrate (see the Supporting Information). [c]PDE1 selectivity factors were calculated by dividing the IC$_{50}$ versus PDE1 by the human PDE9A-IC$_{50}$ (PDE1-IC$_{50}$/PDE9A-IC$_{50}$); see the Supporting Information for details on measurement of IC$_{50}$ versus PDE1; ent: single enantiomer, absolute stereochemistry was not elucidated; rac: racemate.
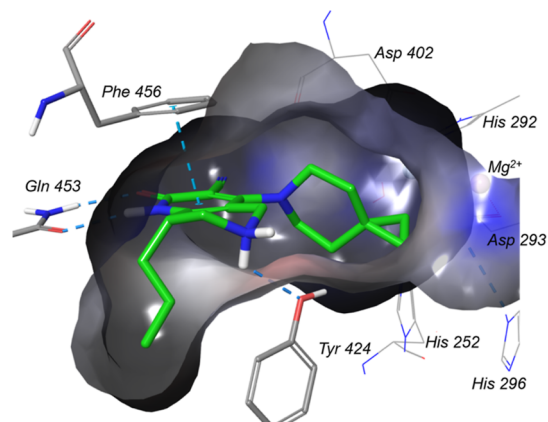

**Figure 7.** Docking of **30** into human PDE9A X-ray (PDB: 3JSW).

administration of 5 or 40 mg/kg BAY-7081, no significant effects on blood pressure and heart rate were observed within 24 h.

PDE9A has been suggested as a regulator of intracellular cGMP levels within the natriuretic peptide [atrial natriuretic peptide (ANP)/brain natriuretic peptide (BNP)] signaling pathway. Compared to sGC stimulation and activation, PDE9A inhibition seems to address an alternate cGMP pool whose modulation has been shown to translate into beneficial effects in a heart disease model in rodents.[11] Based on these findings, the effects of inhibiting PDE9A with PF-04447943 were studied in a mouse myocardial hypertrophy model [transverse aortic constriction (TAC)]. Animals were treated twice daily with 10 mg/kg for 5 weeks. A statistically significant reduction of hypertrophy of the left atrium and a trend for improvement of heart function were observed in PDE9A inhibitor-treated animals (Figure 9). Consistent with improved LVEDP in the treatment group, a reduction in LVPmin was found (see the Supporting Information).

These findings add to the growing body of evidence that PDE9A inhibition might positively impact diseases of the kidney and the heart. However, more studies in relevant disease models are needed to broaden the basis for the connection of PDE9A inhibition and cardiovascular diseases.

■ CONCLUSIONS

We have optimized a weakly active PDE9A HTS hit to a potent, selective, and orally bioavailable PDE9A inhibitor. The key step during the campaign was the exchange of the aromatic head group to an aliphatic piperidine-based moiety that led to a switch from glucuronidation to oxidative metabolism of the cyanopyridone-based lead structure. Changing the metabolic pathway proved essential in identifying inhibitors with improved in vivo PK properties and ultimately BAY-7081. PDE9A inhibition has been suggested as an approach that

Scheme 1. Synthesis of BAY-7081 (30)[a]
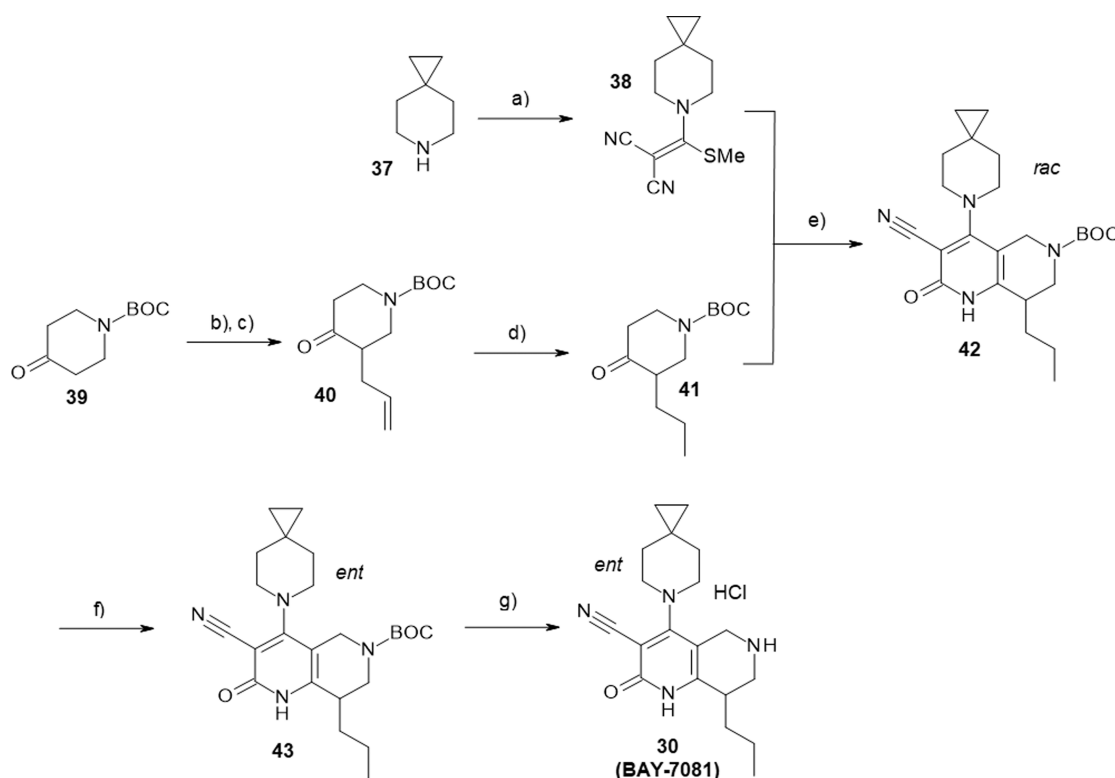
[a]Reagents and conditions: (a) 2-[di(methylthio)methylidene]malodinitrile, triethylamine (TEA), dichloromethane (DCM), reflux, 87%; (b) pyrrolidine, magnesium sulfate, toluene, room temperature (r.t.), overnight; (c) allyl bromide, acetonitrile, r.t., 4 h, 46% over two steps; (d) Pd/C, H$_2$, tetrahydrofurane (THF), r.t., overnight, 99%; (e) cesium carbonate, dimethyl sulfoxide (DMSO), r.t., 48 h and then acetic acid, water, 90 °C, 2 h, 39%; (f) chiral chromatography, eluent CO$_2$/EtOH, 46%, 100% ee; (g) HCl in 1,4-dioxane, DCM, r.t., overnight, 95%. BOC = *tert*-butoxycarbonyl; DCM = dichloromethane; DMSO = dimethyl sulfoxide; EtOH = ethanol; r.t. = room temperature; TEA = triethylamine; and THF = tetrahydrofurane. ent: single enantiomer, absolute stereochemistry was not elucidated; rac: racemate.

Table 6. PDE Selectivity Panel for BAY-7081 (30)

IC$_{50}$ [nM][a]	PDE1[b]	PDE2A[b]	PDE3B[b]	PDE4B[b]	PDE5A[b]	PDE6[b]	PDE7B[b]	PDE8A[b]	PDE10A[b]	PDE11A[b]
15	49x	>650x	>650x	238x	143x	101x	>650x	97x	>650x	430x

[a]IC$_{50}$ versus human PDE9A enzyme, see the Supporting Information. [b]Selectivity factors were calculated by dividing the IC$_{50}$ of a given PDE by the PDE9A-IC$_{50}$ (PDE#-IC$_{50}$/PDE9A-IC$_{50}$), see the Supporting Information for details on IC$_{50}$ measurements.

Table 7. PK Profile of PDE9A Inhibitor BAY-7081 (30) in Selected Species[a]

species	CL$_b$[b] [L h^{-1} kg^{-1}]	V_{SS}[c] [L kg^{-1}]	MRT[d] [h]	F[e] [%]
Rat	2.4	4.5	1.9	61
Dog	0.9	3.0	4.0	80

[a]Values were derived by intravenous (dose 0.3 mg kg^{-1}) and oral (dose 1.0 mg kg^{-1}) administration of solutions in either plasma 99% + DMSO 1% (rat iv) or EtOH/PEG400/H$_2$O (dog iv, rat and dog po) vehicles. [b]Blood clearance. [c]Volume of distribution at steady state. [d]Mean residence time after iv application. [e]Oral bioavailability; see the Supporting Information for details.

Table 8. PK Profile of PDE9A Inhibitor PF-04447943 in Selected Species[a]

species	CL$_b$[b] [L h^{-1} kg^{-1}]	V_{SS}[c] [L kg^{-1}]	MRT[d] [h]	F[e] [%]
rat	3.0	2.2	0.8	41
dog	0.5	1.5	3.1	38

[a]Values were derived by intravenous (dose 0.3 mg kg^{-1}) and oral (dose 3.0 mg kg^{-1} for rat and 1.0 mg kg^{-1} for dog) administration of solutions in either plasma 99% + DMSO 1% (rat iv) or EtOH/PEG400/H$_2$O (dog iv, rat and dog po) vehicles. [b]Blood clearance. [c]Volume of distribution at steady state. [d]Mean residence time after iv application. [e]Oral bioavailability; see the Supporting Information for details.

might be beneficial for heart failure patients, and the pharmacological data shown in this article also point into this direction. With BAY-7081, we have provided a novel chemical tool with high aqueous solubility to assess PDE9A-mediated pharmacology, including those relevant for kidney and heart diseases.

■ EXPERIMENTAL SECTION

Chemistry. General: all commercial reagents and catalysts were used as provided by the commercial supplier without purification. Solvents for synthesis, extraction, and chromatography were of reagent grade and used as received. Moisture-sensitive reactions were carried out under an atmosphere of argon, and anhydrous solvents were used as provided by the commercial supplier. Reaction progress

Table 9. Physicochemistry for BAY-7081 (30)

MW [g/mol][a]	$c \log D^{b}$	HBD[c]	HBA[d]	BEI[e]	LLE[f]	solubility [mg/L][g]
326	2.2	2	4	23.9	6.1	>500

[a]Free base. [b]Calculated for pH 7.5. [c]Number of H-bond donors. [d]Number of H-bond acceptors. [e]Binding efficiency index $-\log (\text{IC}_{50})/\text{MW} \times 1000$. [f]Lipophilic ligand efficiency $-\log (\text{IC}_{50}) - c \log D_{7.5}$. [g]Measured at pH 7 in aqueous buffer from crystalline material (see the Supporting Information).
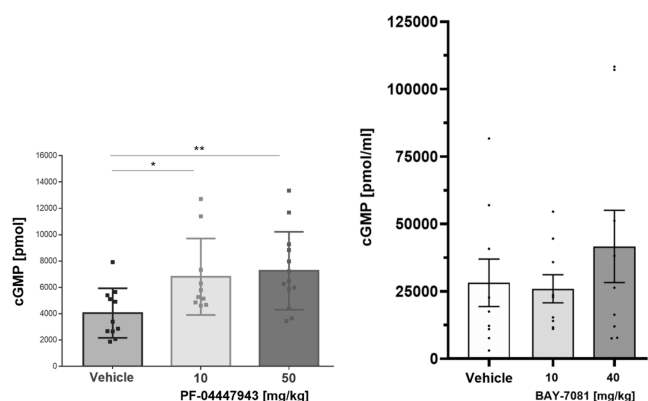

Figure 8. Urinary cGMP levels in rats after PDE9A inhibition (see the Supporting Information for details).

was monitored by high-performance liquid chromatography (HPLC), LC/mass spectrometry (LC/MS), or thin-layer chromatography. Crude products were immediately purified using preparative reversed-phase HPLC methodology with UV detection or flash chromatography on silica gel. The fractions obtained were concentrated in vacuo to remove organic volatiles. Unless otherwise indicated, all compounds have greater than 95% purity. Calculated log $D_{7.5}$ values were determined by use of a novel in silico prediction tool developed in cooperation of Simulation Plus and Bayer. ^{1}H NMR and ^{13}C NMR spectra were recorded in DMSO-d_6 or CDCl$_3$ at RT with Bruker Avance spectrometers operating at 300 or 400 MHz for ^{1}H NMR; at 101 or 126 MHz for ^{13}C NMR. ^{13}C NMR spectra were recorded as broad-band, proton-decoupled spectra. Chemical shifts are reported in parts per million relative to tetramethylsilane as an internal standard. The descriptions of the coupling patterns of ^{1}H NMR signals are based on the optical appearance of the signals and do not necessarily reflect the physically correct interpretation. In general, the chemical shift information refers to the center of the signal. In the case of multiplets, intervals are given. Spin multiplicities are reported

as s = singlet, br s = broad singlet, d = doublet, dd = doublet of doublets, t = triplet, q = quartet, and m = multiplet. The following mass spectrometry methods were used. LC/MS method 1: instrument: Waters Acquity SQD ultra-performance LC (UPLC) System; column: Waters Acquity UPLC HSS T3 1.8 μm 50 × 1 mm; eluent A: 1 L water + 0.25 mL 99% ige formic acid, eluent B: 1 L acetonitrile + 0.25 mL 99% ige formic acid; gradient: 0.0 min 90% A → 1.2 min 5% A → 2.0 min 5% A; oven: 50 °C; flow: 0.40 mL/min; and UV detection: 210 nm. LC/MS method 3: system MS: Thermo Scientific Fourier transform MS (FT-MS); System UHPLC+: Thermo Scientific UltiMate 3000; column: Waters, HSST3, 2.1 × 75 mm, C18 1.8 μm; eluent A: 1 L water + 0.01% formic acid; eluent B: 1 L acetonitrile + 0.01% formic acid; gradient: 0.0 min 10% B → 2.5 min 95% B → 3.5 min 95% B; oven: 50 °C; flow: 0.90 mL/min; and UV detection: 210 nm/optimum integration path 210−300 nm. GC/MS method: instrument: Thermo Scientific DSQII, Thermo Scientific Trace GC Ultra; column: Restek RTX-35MS, 15 m × 200 μm × 0.33 μm; constant flow with helium: 1.20 mL/min; oven: 60 °C; inlet: 220 °C; and gradient: 60 °C, 30 °C/min → 300 °C (3.33 min hold). Single mass analysis (HR-MS): instrument: waters time-of-flight system (ToF) and electrospray ionization (ESI). Quantitative ion chromatography (IC) was performed with external standards on a Thermo Scientific ICS5000+ instrument with capillary IC columns (IonPac AS11-HC and IonPac CS16), eluent gradient $[\text{H}]^+ [\text{OH}]^-$, and conductivity detection. Assessment of optical rotation $[\alpha]$ was performed using an Anton Paar Polarimeter MCP200 with parameters (solvent, wavelength, and temperature) as indicated.

Synthesis of BAY-7081 (30). *tert-Butyl 4-(Pyrrolidin-1-yl)-3,6-dihydropyridine-1(2H)-carboxylate.* *tert*-Butyl-4-oxopiperidine-1-carboxylate **39** (2.0 kg, 10.04 mol) and magnesium sulfate (4.0 kg, 33.23 mol) were suspended in 18.5 L of toluene. Pyrrolidine (2.0 L, 23.99 mol) was added over a period of 30 min. The internal temperature was kept between 10 and 15 °C. Then, the mixture was stirred at 25 °C overnight. Magnesium sulfate was filtered off and washed with toluene, and the filtrate was evaporated on a rotary evaporator. 2.48 kg (98% yield) of the title compound was obtained. GC−MS (ESIpos): m/z = 252 [M]. ^{1}H NMR (400 MHz, CDCl$_3$) δ [ppm] = 4.14 (m, 1H), 3.96 (br s, 2H), 3.72 (t, 1H), 3.53 (t, 1H), 3.04 (m, 3H), 2.85 (m, 1H), 2.44 (m, 1H), 2.26 (m, 1H), 1.82 (m, 3H), 1.70 (m, 1H), and 1.47 (m, 9H).

rac-tert-Butyl 3-Allyl-4-oxopiperidine-1-carboxylate (40). *tert*-Butyl 4-(pyrrolidin-1-yl)-3,6-dihydropyridine-1(2H)-carboxylate (2.48 kg, 9.85 mol) was dissolved in 13.2 L of acetonitrile. At an internal temperature of 20−26 °C, allyl bromide (1.15 L, 9.52 mol) was added dropwise. After 4 h, 2 L of water was added and the reaction mixture was stirred at r.t. overnight. The mixture was poured into 50 L of stirred water and extracted with ethyl acetate. The combined organic layers were concentrated, and the crude product was purified by column chromatography (eluent: 90 L EE/Cy 1:20, 50 L EE/Cy 1:8). 1.12 kg (98% purity, 46% yield) of the title

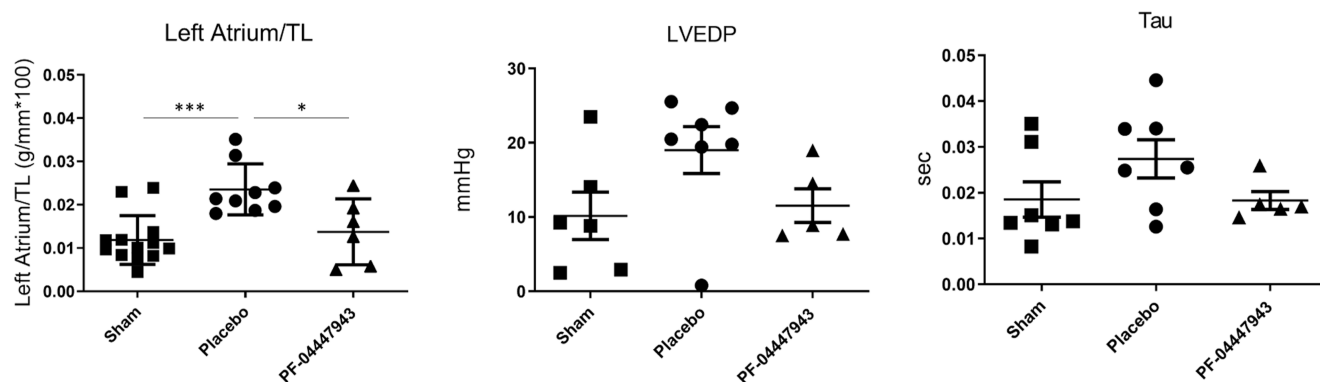**Figure 9.** Effect of PDE9A inhibitor PF-04447943 in the mouse TAC model. Left atrium/TL: weight of left atrium/tibia length; LVEDP: left ventricular end diastolic pressure; and Tau: left ventricular relaxation time constant; $***p = 0.0004$, $*p = 0.0111$, analysis of variance (ANOVA) followed by Dunnett's multiple comparisons test; see the Supporting Information for details on study and additional results.

compound was obtained. GC/MS (ESIpos): m/z = 239 [M]. ^{1}H NMR (400 MHz, CDCl$_3$) δ [ppm] = 5.76 (m, 1H), 5.06 (dd, 2H), 4.05 (m, 1H), 2.56−2.40 (m, 5H), 2.10−2.02 (m, 1H), and 1.60−1.46 (m, 11H).

rac-tert-Butyl-4-oxo-3-propylpiperidine-1-carboxylate (41). *rac-tert*-Butyl 3-allyl-4-oxopiperidine-1-carboxylate **40** (87.0 g, 363.5 mmol) was dissolved in 1 L of THF. Under argon, palladium on activated carbon (3.9 g, 10%, 36.35 mmol) was added to the mixture and the mixture was hydrogenated overnight under normal pressure. The catalyst was filtered off through silica gel and washed with THF. The filtrate was concentrated on a rotary evaporator and the residue was dried in vacuo. 86.5 g (100% purity, 99% yield) of the title compound was obtained. GC/MS (ESIpos): m/z = 241 [M]. ^{1}H NMR (400 MHz, CDCl$_3$) δ [ppm] = 3.74−4.25 (m, 2H), 2.91−3.63 (m, 2H), 2.33−2.50 (m, 3H), 1.64−1.77 (m, 1H), 1.50 (s, 9H), 1.20−1.43 (m, 3H), and 0.93 (t, 3H).

[6-Azaspiro[2.5]octan-6-yl(methylsulfanyl)methylene]-malononitrile (38). [*bis*(Methylsulfanyl)methylidene]-propanedinitrile (182.58 g, 1.07 mol) and 6-azaspiro[2.5]octane hydrobromide (206 g, 1.07 mol) were dissolved in 2.3 l of DCM. Triethylamine (164.4 mL, 1.18 mol) was added, and the mixture was refluxed overnight. The solvent was removed on a rotary evaporator, and the residue was diluted with 3 L of di-isopropyl ether and 1.5 L of petroleum ether. The precipitated solid was filtered off, washed with di-isopropyl ether/petroleum ether 2:1, and dried in vacuo. 218 g (100% purity, 87% yield) of the title compound was obtained. LC−MS method 3 (ESIpos): m/z = 234 [M + H]$^+$. ^{1}H NMR (400 MHz, DMSO-d_6): δ [ppm] = 3.76 (dd, 4H), 2.54 (s, 3H), 1.51 (dd, 4H), and 0.41 (s, 4H).

rac-tert-Butyl-4-(6-azaspiro[2.5]octan-6-yl)-3-cyano-2-oxo-8-propyl-1,5,7,8-tetrahydro-1,6-naphthyridine-6(2H)-carboxylate (42). Cesium carbonate (33.06 g, 101.5 mmol) was suspended in 190 mL of DMSO. *Rac-tert*-Butyl-4-oxo-3-propylpiperidine-1-carboxylate **41** (19.59 g, 81.17 mmol) was added, and the mixture was stirred 20 min at r.t. before [6-azaspiro[2.5]octan-6-yl(methylsulfanyl)-methylene]malononitrile **38** (9.47 g, 40.59 mmol) was added. The mixture was stirred for 48 h at r.t.. Then, 90 mL of water and 45 mL of acetic acid were added and the reaction mixture was stirred for 2 h at 100 °C. After cooling to r.t., the precipitated solid was filtered off, washed with *tert*-butyl methyl ether (MTBE), and dried in vacuo. 6.71 g (100% purity, 39% yield) of the title compound was obtained. LC−MS method 3 (ESIpos): m/z = 427 [M + H]$^+$. ^{1}H NMR (400 MHz, DMSO-d_6) δ [ppm] = 11.75 (br s, 1H), 4.47 (m, 1H), 3.95 (m, 2H), 3.12 (m, 1H), 1.20−1.64 (m, 19H), 0.89 (br d, 5H), and 0.38 (s, 5H).

ent-tert-Butyl-4-(6-azaspiro[2.5]octan-6-yl)-3-cyano-2-oxo-8-propyl-1,5,7,8-tetrahydro-1,6-naphthyridine-6(2H)-carboxylate (43). Enantiomeric separation of 8.2 g of (19.22 mmol) *rac-tert*-butyl-4-(6-azaspiro[2.5]octan-6-yl)-3-cyano-2-oxo-8-propyl-1,5,7,8-tetrahydro-1,6-naphthyridine-6(2H)-carboxylate **42** was done using the following preparative chiral HPLC method: machine THAR SFC-Super Chrom Prep 200; column Chiralpak AD-H (SFC) 5 μm 250 × 30 mm; solvent 86% CO$_2$/14% ethanol; flow 175 mL/min; pressure 135 bar; temperature eluent 38 °C; temperature Zyklon 70 °C; pressure Zyklon 24 bar; column temperature 38 °C; and UV detection 210 nm. Product-containing samples were united, and the solvents were evaporated. 3.78 g (100% purity, 46% yield) of the title compound was obtained. Chiral HPLC (Agilent SFC column: Chiralpak AD-3, 3 μm, 100 × 4.6 mm; solvent: 80% CO$_2$/20% ethanol; BPR pressure: 130 bar, BPR temperature: 60 °C, column temperature: 40 °C; flow: 3 mL/min; and UV detection: 210 nm): 100% ee. LC−MS method 1 (ESIpos): m/z = 427 [M + H]$^+$. ^{1}H NMR (400 MHz, DMSO-d_6): δ [ppm] = 11.75 (s, 1H), 4.28−4.55 (m, 1H), 3.73−4.16 (m, 2H), 3.32−3.44 (m, 2H), 3.31 (m, 3H), 2.95−3.21 (m, 1H), 2.56−2.71 (m, 1H), 1.41 (s, 16H), 0.89 (br s, 3H), and 0.38 (s, 4H).

ent-4-(6-Azaspiro[2.5]octan-6-yl)-2-oxo-8-propyl-1,2,5,6,7,8-hexahydro-1,6-naphthyridine-3-carbonitrile Hydrochloride (30). *ent-tert*-Butyl-4-(6-azaspiro[2.5]octan-6-yl)-3-cyano-2-oxo-8-propyl-1,5,7,8-tetrahydro-1,6-naphthyridine-6(2H)-carboxylate **43** (22.5 g,

52.75 mmol) was dissolved in 1 L of DCM. HCl in dioxane (131.87 mL, 4.0 M, 527.47 mmol) was added, and the mixture was stirred at r.t. overnight. The reaction mixture was concentrated on a rotary evaporator, and the residue was stirred in 750 mL of acetonitrile. The solid was filtered off, washed two times with each 50 mL of acetonitrile, and dried at 60 °C bath temperature on a rotary evaporator. 18.1 g (100% purity; 95% yield) of the title compound was obtained. LC−MS method 3 (ESIpos): m/z = 327 [M + H]$^+$. ^{1}H NMR (400 MHz, DMSO-d_6): δ [ppm] = 11.72−11.94 (s, 1H), 8.67−9.85 (m, 2H), 3.86−4.03 (m, 2H), 3.44−3.57 (m, 1H), 3.34−3.44 (m, 4H), 2.81−3.08 (m, 2H), 1.37−1.79 (m, 6H), 1.19−1.34 (m, 2H), and 0.88 (s, 3H), 0.39 (s, 4H). ^{13}C NMR (126 MHz, DMSO-d_6): δ [ppm] = 164.61, 161.92, 148.17, 116, 97, 103.53, 87.91, 50.98, 43.27, 40.92, 34.73, 33.83, 33.49, 18.48, 16.90, 13.59, and 10.97. HRMS m/z: [M + H]$^+$ calcd for C$_{19}$H$_{27}$N$_4$O, 327.2185; found, 327.2190. $[\alpha]_D^{20}$ = −186.4° (in methanol, 20.0 °C, 589 nm). Ion chromatography: w(Cl$^-$) = 10, 7 wt % = 1 equiv (Cl$^-$). Chiral HPLC (Column: ChiralTek AD-3 3 μm 50 × 4.6 mm; solvent: 50% iso-hexane/50% ethanol + 0.2% DEA; flow: 1 mL/min; and UV detection: 220 nm): R_t = 4.933 min, 99.0% ee.

■ ASSOCIATED CONTENT

ⓢ Supporting Information

The Supporting Information is available free of charge at https://pubs.acs.org/doi/10.1021/acs.jmedchem.2c01267.

■ AUTHOR INFORMATION

Corresponding Author

Daniel Meibom − *Bayer AG, 42113 Wuppertal, Germany;* ⦿ orcid.org/0000-0003-4978-9842; Email: daniel.meibom@bayer.com

Authors

Sina Micus − *Bayer AG, 42113 Wuppertal, Germany*

Anna Lena Andreevski − *Bayer AG, 42113 Wuppertal, Germany*

Sonja Anlauf − *Bayer AG, 42113 Wuppertal, Germany*

Pamela Bogner − *Bayer AG, 42113 Wuppertal, Germany;* Present Address: Amgen Research (Munich) GmbH, Staffelseestr. 2, 81477 München, Germany

Clemens-Jeremias von Buehler − *Bayer AG, 42113 Wuppertal, Germany*

André P. Dieskau − *Bayer AG, 42113 Wuppertal, Germany*

Jan Dreher − *Bayer AG, 42113 Wuppertal, Germany*

Frank Eitner − *Bayer AG, 42113 Wuppertal, Germany*

Daniela Fliegner − *Bayer AG, 42113 Wuppertal, Germany;* Present Address: Pfizer Pharma GmbH, Linkstraße 10, 10785 Berlin, Germany

Markus Follmann − *Bayer AG, 42113 Wuppertal, Germany;* ⦿ orcid.org/0000-0003-1246-3603

Kersten Matthias Gericke − *Bayer AG, 42113 Wuppertal, Germany*

Stefanie Maassen − *Bayer AG, 42113 Wuppertal, Germany*

Jutta Meyer − *Bayer AG, 42113 Wuppertal, Germany*

Karl-Heinz Schlemmer − *Bayer AG, 42113 Wuppertal, Germany*

Holger Steuber − *Bayer AG, 13353 Berlin, Germany;* Present Address: Nuvisan Innovation Campus Berlin GmbH, 13353 Berlin, Germany

Adrian Tersteegen − *Bayer AG, 42113 Wuppertal, Germany*

Frank Wunder − *Bayer AG, 42113 Wuppertal, Germany*

Complete contact information is available at:
https://pubs.acs.org/10.1021/acs.jmedchem.2c01267

Author Contributions

The manuscript was written with contributions from all authors. All authors have given approval to the final version of the manuscript.

Notes

The authors declare the following competing financial interest(s): All authors have been employees of Bayer AG during the course of the project.

■ ABBREVIATIONS

ANOVA, analysis of variance; ANP, atrial natriuretic peptide; Asn, asparagine; BEI, binding efficiency index; BNP, brain natriuretic peptide; cGMP, cyclic guanosine monophosphate; BOC, *tert*-butoxycarbonyl; Cl, clearance; CNS, central nervous system; CYP, cytochrome P enzyme; d, doublet (in NMR); DCM, dichloromethane; dd, doublet of doublets (in NMR); DMSO, dimethyl sulfoxide; ee, enantiomeric excess; EE, ethyl acetate; EI, electron ionization; ent, single enantiomer; EtOH, ethanol; F, bioavailability; GC, gas chromatography; Gln, glutamine; HBA, number of H-bond acceptors; HBD, number of H-bond donors; hERG, human ether-a-go-go channel; HFpEF, heart failure with preserved ejection fraction; HFrEF, heart failure with reduced ejection fraction; HPLC, high-performance liquid chromatography; HTS, high-throughput screening; HW, heart weight; IC_{50}, concentration leading to 50% inhibition; iv, intravenous; LLE, lipophilic ligand efficiency; LVP, left ventricular pressure; m, multiplet (in NMR); M, molar; μM, micromolar; MRT, mean residence time; MS, mass spectrometry; MTBE, *tert*-butyl methyl ether; MW, molecular weight; nM, nanomolar; NMR, nuclear magnetic resonance; NO, nitric oxide; PDB, protein data bank; PDE, phosphodiesterase; PEG, polyethylene glycol; Phe, phenylalanine; PK, pharmacokinetic; pmol, picomol; po, per os; ppm, parts per million (in NMR); q, quartet (in NMR); rac, racemate; r.t., room temperature; s, singlet (in NMR); SAR, structure−activity relationship; SFC, supercritical fluid chromatography; sGC, soluble guanylate cyclase; t, triplet (in NMR); TAC, transverse aortic constriction; TEA, triethylamine; THF, tetrahydrofurane; TL, tibia length; Tyr, tyrosine; V_{ss}, volume of distribution at steady state

■ REFERENCES

(1) Friebe, A.; Sandner, P.; Schmidtko, A. cGMP: A unique 2nd messenger molecule − recent developments in cGMP research and development. *Naunyn-Schmiedeberg's Arch. Pharmacol.* **2020**, *393*, 287−302.

(2) Maurice, D.; Ke, H.; Ahmad, F.; Wang, Y.; Chung, J.; Manganiello, V. C. Advances in targeting cyclic nucleotide phosphodiesterases. *Nat. Rev. Drug Discov.* **2014**, *13*, 290−314.

(3) Omori, K.; Kotera, J. Overview of PDEs and their regulation. *Circ. Res.* **2007**, *100*, 309−327.

(4) Harms, J. F.; Menniti, F. S.; Schmidt, C. J. Phosphodiesterase 9A in brain regulates cGMP signaling independent of nitric-oxide. *Front. Neurosci.* **2019**, *13*, 837.

(5) Brady, S.; Siegel, G.; Albers, R. W.; Price, D. *Basic Neurochemistry*, 7th ed.; eBook, 2005.

(6) Shao, Y. X.; Huang, M.; Cui, W.; Feng, L. J.; Wu, Y.; Cai, Y.; Li, Z.; Zhu, X.; Liu, P.; Wan, Y.; Ke, H.; Luo, H. B. Discovery of a phosphodiesterase 9A inhibitor as a potential hypoglycemic agent. *J. Med. Chem.* **2014**, *57*, 10304−10313.

(7) Patel, N. S.; Klett, J.; Pilarzyk, K.; Lee, D.; Kass, D.; Menniti, F. S.; Kelly, M. P. Identification of new phosphodiesterase 9A (PDE9A) isoforms and how their expression and subcellular compartmentalization in brain changes across the lifespan. *Neurobiol. Aging* **2018**, *65*, 217−234.

(8) Wang, P.; Wu, P.; Egan, R. W.; Billah, M. Identification and characterization of a new human type 9 cGMP-specific phosphodiesterase splice variant (PDE9A5): differential tissue distribution and subcellular localization of PDE9A variants. *Gene* **2003**, *314*, 15−27.

(9) Soderling, S. H.; Bayuga, S. J.; Beavo, J. A. Identification and characterization of a novel family of cyclic nucleotide phosphodiesterases. *J. Biol. Chem.* **1998**, *273*, 15553−15558.

(10) Lakics, V.; Karran, E. H.; Boess, F. G. Quantitative comparison of phosphodiesterase mRNA distribution in human brain and peripheral tissues. *Neuropharm* **2010**, *59*, 367−374.

(11) Lee, D. I.; Zhu, G.; Sasaki, T.; Cho, G. S.; Hamdani, N.; Holewinski, R.; Jo, S. H.; Danner, T.; Zhang, M.; Rainer, P. P.; Bedja, D.; Kirk, J. A.; Ranek, M. J.; Dostmann, W. R.; Kwon, C.; Margulies, K. B.; Van Eyk, J. E.; Paulus, W. J.; Takimoto, E.; Kass, D. A. Phosphodiesterase 9A controls nitric-oxide-independent cGMP and hypertrophic heart disease. *Nature* **2015**, *519*, 472−476.

(12) Shen, K.; Johnson, D. W.; Gobe, Gl. C. The role of cGMP and its signaling pathways in kidney disease. *Am. J. Physiol. Ren. Physiol.* **2016**, *311*, F671−F681.

(13) Chen, Y.; Burnett, J. C. Particulate guanylyl cyclase A/cGMP signaling pathway in the kidney: physiologic and therapeutic indications. *Int. J. Mol. Sci.* **2018**, *19*, 1006.

(14) Park, M.; Sandner, P.; Krieg, T. cGMP at the centre of attention: emerging strategies for activating the cardioprotective PKG pathway. *Basic Res. Cardiol.* **2018**, *113*, 24.

(15) Greene, S. J.; Gheorghiade, M.; Borlaug, B. A.; Pieske, B.; Vaduganathan, M.; Burnett, J. C.; Roessig, L.; Stasch, J.-P.; Solomon, S. D.; Paulus, W. J.; Butler, J. The cGMP signaling pathway as a therapeutic target in heart failure with preserved ejection fraction. *J. Am. Heart Assoc.* **2013**, *2*, No. e000536.

(16) Monica, F. Z.; Murad, F.; Bian, K. Modulating cGMP levels as therapeutic drug targets in cardiovascular and non-cardiovascular diseases. *OA Biochem.* **2014**, *2*, 3.

(17) Schlossmann, J.; Schinner, E. cGMP becomes a drug target. *Naunyn-Schmiedeberg's Arch. Pharmacol.* **2012**, *385*, 243−252.

(18) McArthur, J. G.; Svenstrup, N.; Chen, C.; Fricot, A.; Carvalho, C.; Nguyen, J.; Nguyen, P.; Parachikova, A.; Abdulla, F.; Vercellotti, G. M.; Hermine, O.; Edwards, D.; Ribeil, J.-A.; Belcher, J. D.; Maciel, T. T. A novel, highly potent and selective phosphodiesterase-9 inhibitor for the treatment of sickle cell disease. *Haematologica* **2020**, *105*, 623−631.

(19) Tuttle, J. B.; Kormos, B. L. The use of PDE10A and PDE9 Inhibitors for treating schizophrenia. *Top. Med. Chem.* **2015**, *13*, 255−316.

(20) Menniti, F. S.; Plath, N.; Svenstrup, N.; Schmidt, C. J. Pharmacological manipulation of cyclic nucleotide phosphodiesterase signaling for the treatment of neurological and psychiatric disorders in the brain. *Cyclic-Nucleotide Phosphodiesterases In The Central Nervous System*; John Wiley & Sons, 2014; Chapter 4.

(21) Wu, Y.; Li, Z.; Huang, Y.-Y.; Wu, D.; Luo, H.-B. Novel phosphodiesterase inhibitors for cognitive improvement in alzheimer's disease. *J. Med. Chem.* **2018**, *61*, 5467−5483.

(22) Kumar, A. K.; Forslund, R. E.; Cardurion Pharmaceuticals. Meglumine salts of thienopyrimidines. WO 2019204298 A1, 2019.

(23) Mendelsohn, M. E.; Cardurion Pharmaceuticals. Methods for treatment of heart failure, WO 2018009899 A1, 2018.

(24) Wunder, F.; Tersteegen, A.; Rebmann, A.; Erb, C.; Fahrig, T.; Hendrix, M. Characterization of the first potent and selective PDE9 inhibitor using a cGMP reporter cell line. *Mol. Pharmacol.* **2005**, *68*, 1775−1781.

(25) Verhoest, P. R.; Fonseca, K. R.; Hou, X.; Proulx-LaFrance, C.; Corman, M.; Helal, C. J.; Claffey, M. M.; Tuttle, J. B.; Coffman, K. J.; Liu, S.; Nelson, F.; Kleiman, R. J.; Menniti, F. S.; Schmidt, C. J.; Vanase-Frawley, M.; Liras, S. Design and discovery of 6-[(3S,4S)-4-Methyl-1-(pyrimidin-2-ylmethyl)pyrrolidin-3-yl]-1-(tetrahydro-2H-pyran-4-yl)-1,5-dihydro-4H-pyrazolo[3,4-d]pyrimidin-4-one (PF-04447943), a selective brain penetrant PDE9A inhibitor for the treatment of cognitive disorders. *J. Med. Chem.* **2012**, *55*, 9045−9054.

(26) Rosenbrock, H.; Giovannini, R.; Schänzle, G.; Koros, E.; Runge, F.; Fuchs, H.; Marti, A.; Reymann, K. G.; Schröder, U. H.; Fedele, E.; Dorner-Ciossek, C. The novel phosphodiesterase 9A inhibitor BI 409306 increases cyclic guanosine monophosphate levels in the brain, promotes synaptic plasticity, and enhances memory function in rodents. *J. Pharmacol. Exp. Ther.* **2019**, *371*, 633−641.

(27) Converso, A.; Rodzinak, K. J.; Merck Sharp & Dohme Corp. Aza-cyanoquinolinone PDE9 inhibitors. WO 2017019723 A1, 2017.

(28) Wu, F.; Li, L.; Yang, X.; Transthera Biosciences Co. LTD.PDE9 inhibitor and use thereof. WO 2020151636 A1, 2019.

(29) Tominaga, Y.; Kawabe, M.; Hosomi, A. Synthesis of 4-methylthio-2(1H)-pyridone derivatives using ketene dithioacetals. *J. Heterocycl. Chem.* **1987**, *24*, 1325−1331.

(30) Ren, Q.; Mo, W.; Gao, L.; He, H.; Gua, Y. Facile synthesis and herbicidal activity of novel multisubstituted pyridine derivatives. *J. Heterocycl. Chem.* **2010**, *47*, 171−178.

(31) Charnigo, R. J.; Beidler, D.; Rybin, D.; Pittman, D. D.; Tan, B.; Howard, J.; Michelson, A. D.; Frelinger, A. L.; Clarke, N. PF-04447943, a phosphodiesterase 9A inhibitor, in stable sickle cell disease patients: a phase Ib randomized, placebo-controlled study. *Clin. Transl. Sci.* **2019**, *12*, 180−188.

(32) Priksz, D.; Bombicz, M.; Varga, B.; Kurucz, A.; Gesztelyi, R.; Balla, J.; Toth, A.; Papp, Z.; Szilvassy, Z.; Juhasz, B. Upregulation of myocardial and vascular phosphodiesterase 9A in a model of atherosclerotic cardiovascular disease. *J. Mol. Sci.* **2018**, *19*, 2882.

(33) Scott, N. J. A.; Rademaker, M. T.; Charles, C. J.; Espiner, E. A.; Richards, A. M. Hemodynamic, Hormonal, and renal actions of phosphodiesterase-9 inhibition in experimental heart failure. *J. Am. Coll. Cardiol.* **2019**, *74*, 889−901.

(34) Richards, D. A.; Aronovitz, M. J.; Liu, P.; Martin, G. L.; Tam, K.; Pande, S.; Karas, R. H.; Bloomfield, D. M.; Mendelsohn, M. E.; Blanton, R. M. CRD-733, a novel PDE9 (phosphodiesterase 9) inhibitor, reverses pressure overload−induced heart failure. *Circ.: Heart Failure* **2021**, *14*, No. e007300.

(35) Sheng, Z.; Qiang, X.; Li, G.; Wang, H.; Dong, W.; Wu, F. TT-00920, a clinical stage novel phosphodiesterase 9 inhibitor, protects against heart failure in a rat model of myocardial infarction. *Circulation* **2020**, *142*, A13810.

(36) Hamdani, N.; Kovács, Á.; Herwig, M.; Lyu, Y.; Alidadiani, N.; van Linthout, S.; Tschöpe, C.; Bagi, Z.; Hamdani, N. Endothelial and cardiomyocyte dysfunction in heart failure with preserved ejection fraction is attenuated via PDE9A inhibition. *Clin. Res. Cardiol.* **2020**, *68*, S1.

(37) Mishra, S.; Sadagopan, N.; Dunkerly-Eyring, B.; Rodriguez, S.; Sarver, D. C.; Ceddia, R. P.; Murphy, S.; Knutsdottir, H.; Jani, V.; Ashok, D.; Oeing, C. U.; O'Rourke, B.; Gangoiti, J.; Sears, D. D.; Wong, G. W.; Collins, S.; Kass, D. A. Inhibition of phosphodiesterase type 9 reduces obesity and cardiometabolic syndrome in mice. *J. Clin. Invest.* **2021**, *131*, No. e148798.